GMR
The Original

MOLECULAR DOCKING INTERACTION STUDY OF BROMOPHENOLS ISOLATED FROM POLYSIPHONIA SPECIES A RED SEAWEED ON THE KEAP1-KELCH DOMAIN AS FREE RADICAL SCAVENGERS

R. Choudhury [1], N. Sahoo[2], N. R. Kar[3]*

[1]School of Pharmacy and Life Sciences, Centurion University of Technology and Management, Odisha, India, Email: reshmachoudhury43@gmail.com
[2]Nityananda College of Pharmacy, Shergarh, Balasore, Odisha, India, Email: ncpnityananda@gmail.com
[3]School of Pharmacy and Life Sciences, Centurion University of Technology and Management, Odisha, India, Email: nihar_795@rediffmail.com
*Corresponding Author E-mail: nihar_795@rediffmail.com

ABSTRACT
Several bromophenolic compounds from Polysiphonia species across the world have been isolated and structurally elucidated, and their free radical scavenging activity was proven by the DPPH method. Free radicals are formed due to the oxidative stress that the human body suffers due to several reasons. The NRF2 protein system acts as a principal transcription factor that functions as the body's primary protector against oxidative stress. But during unstressed conditions, NRF2 is regulated by its inhibitor, KEAP1 (Kelch-like ECH-associated protein 1). KEAP1 functions as a detector, perpetually attaching to NRF2 and designating it for elimination by the cell's "recycling mechanism." If this protein-protein interaction can be inhibited by small molecule inhibitors, then the body's free radical scavenging potential can remain switched on, and the body can be freed from this harmful free radical. Herein, we have reported the molecular docking study of seventeen compounds (CPD-1 through CPD-17) as polybromophenolic compounds having DPPH activity mentioned as IC_{50} (in µM). AutoDock tools along with CB-Dock2 were employed for docking interaction studies, and four compounds (CPD-16, 10, 14, and 1) were chosen as good hits for this study. The non-bonded interaction studies have identified CPD-16 as the best result, which outperforms in silico data with that of the co-crystallized compound. The binding affinity was found to be -11.0 kcal/mol and has all the crucial interactions with the amino acid residues of the target protein. The common feature pharmacophore implies that the number and position of the bromine atoms in the compounds are crucial along with the scaffold type that hogs the active site of the protein.

KEYWORDS: NRF2, KEAP1, DPPH, Molecular docking, Polysiphonia, Bromophenols

1. INTRODUCTION

The cells within our body continually metabolize food and oxygen, generating energy for bodily functions, alongside byproducts such as metabolites or undigested materials, while also producing detrimental free radicals or superoxide ions (reactive oxygen species, or ROS) **(1, 2)**. The produced free radicals are ephemeral and extremely reactive, and they are chemically neutralized by the antioxidants found in the body **(3,4)**. Conversely, byproducts including oxidized cell membranes, degraded proteins, and metabolic waste (such as carbon dioxide, ammonia, and oxidized cholesterol) are eliminated from the body through various significant cellular mechanisms like autophagy, the Ubiquitin-Proteasome System, efflux transporters, exocytosis, and efferocytosis/phagocytosis **(5, 6)**. Any disruption in cellular equilibrium induces a state of oxidative stress in the body, leading to the generation of harmful free radicals that exceed the body's capacity to counteract them and mend the ensuing damage **(7, 8)**. Mitochondria serve as the primary source of reactive oxygen species during ATP synthesis; however, oxidative stress may also arise from many cellular compartments and external factors **(9)**. Unregulated oxidative stress in humans may lead to medical conditions such as cancer, Alzheimer's disease, Parkinson's disease, myocardial infarctions and strokes, persistent hypertension, type 2 diabetes, chronic renal disease, non-alcoholic fatty liver disease, cataracts, age-related macular degeneration, osteoporosis, among others **(10, 11)**.

In this regard, it is important to note that a comprehensive defense mechanism operates inside this cellular milieu, specifically the NRF2 protein system (Nuclear Factor Erythroid 2-related factor 2, alternatively referred to as NFE2L2). It serves as a principal transcription factor that functions as the body's primary protector against oxidative stress. It regulates the production of more than 200 genes that safeguard cells against oxidative harm **(12)**. In typical, unstressed circumstances, NRF2 is regulated by its inhibitor, KEAP1 (Kelch-like ECH-associated protein 1). KEAP1 functions as a detector, perpetually attaching to NRF2 and designating it for elimination by the cell's "recycling mechanism" (the proteasome) **(13)**. When reactive oxygen species (ROS) or other toxins overwhelm the cells, they emit a distress signal that impacts KEAP1, resulting in a modification of KEAP1's structure. This inhibits the tagging of NRF2 for elimination. The freshly synthesized NRF2 can subsequently accumulate, proceed to the nucleus, and activate its protective genes **(14)**. It activates more than 200 genes capable of synthesizing SODs (superoxide dismutase), catalase, and GPX (glutathione

peroxidase), enhancing the production of fresh glutathione, and augmenting glucose metabolism to supply the essential raw materials (NADPH) required for the regeneration of consumed antioxidants **(15, 16)**.

This current study relates to our previous investigations published on *Polysiphonia subtilissima*, wherein we demonstrated that the methanolic extract of the species exhibits free radical scavenging activity assessed through the DPPH free radical scavenging method **(17, 18, 19).** Based on our prior understanding, numerous bromophenolic compounds have been extracted, their structures defined and they have undergone evaluation for DPPH scavenging action. We have compiled structural information from various research papers regarding bromophenols extracted from multiple species of Polysiphonia and their free radical scavenging efficacy (IC_{50} in µM) as determined by the DPPH assay **(20, 21, 22, 23, 24)**. The objective of evaluating the active compounds is to potentially identify novel pharmacophores from these structures, which could facilitate the discovery of new medications like anticancer agents, antihypertensives, or antidiabetics, representing a significant focus in contemporary drug discovery.

2. MATERIALS AND METHODS

2.1. Materials

The 2D structure of the compounds were drawn from ChemDraw Ultra 12.0 **(25)**. The 2D-descriptors were calculated from SwissADME to check whether the compounds comply Rule Of five (RO5) **(26, 27).** The 3D-crystal structure of KEAP1-KELCH domain was imported from Brook heavens protein data bank (https://www.rcsb.org/) with the accession code: 4IQK **(28)**. The protein and the ligands were prepared by AutoDockTools v4.2 **(29)**. For molecular docking studies CB-Dock2 server was utilized **(30)**. This server can predict the binding sites on protein structure and binding affinity for the ligands for specific sites. CB-Dock2 is an improved version of the protein-ligand blind docking tool that inherits the curvature-based cavity detection procedure and the AutoDock Vina-based molecular docking procedure.

2.2. Methods

2.2.1. Retrieving crystallographic information's from 4IQK complex (28, 31)

In the current investigation, we have chosen Kelch-like ECH-associated protein 1 (KEAP1) or the Kelch/DCH domain (PDB accession code: 4QIK) as the target protein for the molecular docking. This domain facilitates protein-protein interactions (PPI) and primarily functions to associate with the NRF2 transcription factor (notably the ETGE motif) to enhance NRF2 ubiquitination and degradation in typical circumstances. The protein features a high-resolution crystal structure (1.97Å) that delivers precise side-chain configurations. The source of protein is *Homo sapiens*, expressed in the *E. coli* BL21(DE3) type strain. This protein structure includes a docked small-molecule inhibitor, N,N′-Naphthalene-1,4-diylbis(4-methoxybenzenesulfonamide), that competitively obstructs NRF2 binding **(Fig.1)**.

The topography of the Kelch domain adopts a six-bladed β-propeller tertiary structure. Each blade consists of a four-stranded antiparallel β-sheet (strands A, B, C, and D). These six blades are arranged circularly around a central axis, creating a "tunnel" shape **(Fig.1)**. The binding pocket is located on the upper face of this tunnel, formed by the loops connecting the β-strands. The top face is relatively flat but contains distinct grooves (the P1-P5 sub-pockets) that accommodate the specific side chains of the ligand/NRF2.

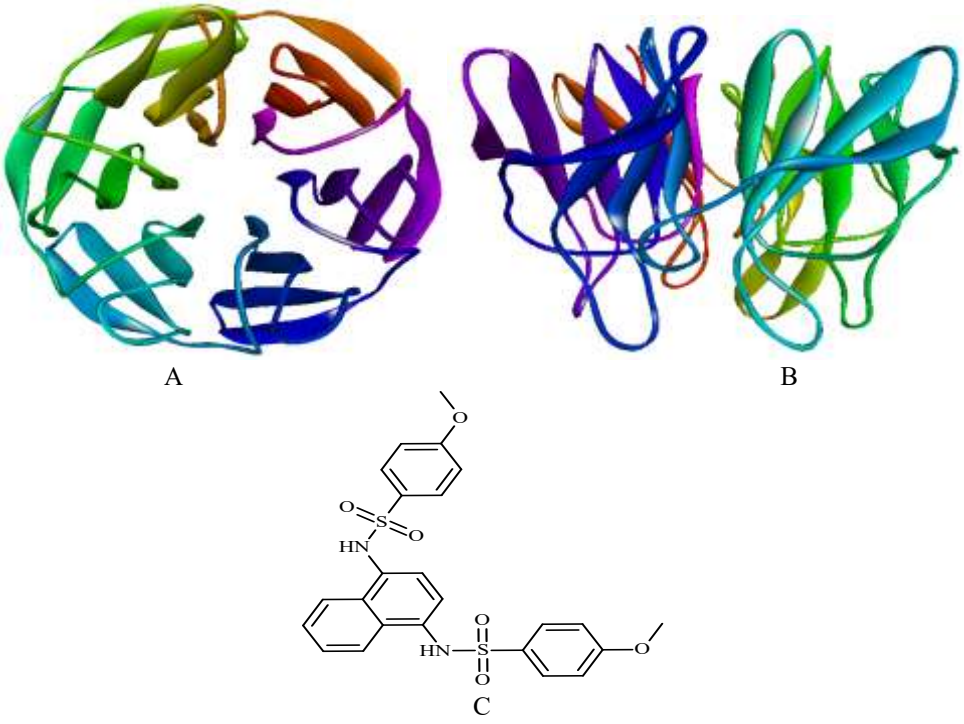

Fig. 1. A. Kelch domain adopts a six-bladed β-propeller tertiary structure; **B.** Four-stranded antiparallel β-sheet; **C.** co-crystallized ligand **(CPD-19)** from PDB ID 4IQK.

The NRF2 binding pocket looks like a hollow central cavity located on the top face of the propeller. It is divided into five sub-pockets (P1 to P5) that recognize the ETGE motif of NRF2. In the following table the precise topographical map of these sub-pockets and their key residues are described in the following table **(Table.1)**.

Table: 1. Critical residues and property of the five sub-pockets of NRF2 binding pocket

Sub-pocket	Charge/Property	Critical Residues (Directly interacting with ligands)
P1	Positively charged (Cationic)	Arg415, Arg483, Ser508, Ile461, Gly462, Phe478
P2	Positively charged (Cationic)	Arg380, Ser363, Asn382, Asn414
P3	Neutral / Polar	Ser602, Ser555, Gly509, Ala556, Gly571, Gly603
P4	Aromatic / Hydrophobic	Tyr572, Gln530, Tyr525
P5	Aromatic / Hydrophobic	Phe577, Tyr334

The most critical feature of this binding site is the formation of the "Arginine Triad" (the hotspot). The residues Arg415, Arg483, and Arg380 form strong cation-π interactions and salt bridges with the acidic glutamate (E) residues of the NRF2 ETGE motif. Any successful inhibitor must engage with at least Arg415 and Arg483 to achieve nanomolar affinity.
From the literature, the binding mode of the co-crystallized ligand shows binding energy as ~10.11 kcal/mol (in silico calculation) with high reproducibility of binding pose with lower RMSD 0.681 Å (RMSD < 2 Å). Specific interactions of the ligand and the binding site receptor atoms were observed. The sulfonamide aromatic rings stack directly against the positively charged guanidinium group of Arg415, forming the cation-π interaction. The naphthalene core forms a strong face-to-face π-π stacking interaction with Tyr525. The sulfonamide oxygens act as acceptors, forming H-bonds with the backbone NH of Ser508 and the side-chain hydroxyls of Ser602 and Ser555. The methoxy groups occupy the hydrophobic P4/P5 sub-pockets, interacting with Phe577 and Tyr572, forming weak Van der Waals interactions.

2.2.2. Developing molecular docking protocol and running protocol (29)
For performing molecular docking of the selected bromophenols with the target proteins, a docking protocol was prepared. This docking procedure is validated after running few cycles of docking.

Step 1: Protein Preparation: The 4IQK.pdb protein file was downloaded from RCSB. All the water molecules and the co-crystallized ligand were removed. Polar hydrogens and Gasteiger charges were added to the protein. The protein structure was optimized by assigning the bond orders and fixing any missing side-chain atoms using the protein preparation wizard in AutoDock Tools 4.2.

Step 2: Ligand Preparation
The bromophenol structures were drawn in ChemBio 3D Ultra 12.0. Energy minimization was performed (MMFF94) to find the global minimum conformation **(Table. 2).** The protonation states were calculated; the torsional values were set at default. The ligands were imported to the working space for further studies.

Step 3: Defining Grid Box
In the AutoGrid procedure the protein is embedded in a 3-D grid and a probe atom is placed at each grid point. The energy of interaction of this single atom with the protein is assigned to the grid point. The centroid of the co-crystallized ligand was chosen as the center of the grid box. XYZ coordinates were fixed at X = 26, Y = 24, and Z = 20. The box dimension was set at 25 Å × 25 Å × 25 Å to ensure that the bromine atoms, which are large, can explore the hydrophobic crevices at the active site.

4. Docking Settings: AutoDock Vina was used for running the docking process. Exhaustiveness was set at 32, which controls the thoroughness of the global search. Higher values increase the chance of finding the true global energy minimum (best binding pose) but require more computational time. The default is 8; 32 is a good choice for more accurate and reproducible results. The number of binding modes was set to nine i.e., maximum number of binding modes (poses) to output. Vina reports these from best (lowest energy) to worst. A random seed number was chosen for generation of random number of poses. The vina default scoring function was used to evaluate the binding affinity (in Kcal/mol).

Table. 2. 2D-Structure of the compounds under study

Compound ID (Ref)	Structures	Compound ID (Ref)	Structures
CPD-1 (20)	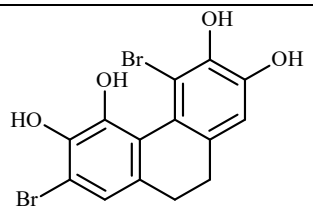	**CPD-2 (20)**	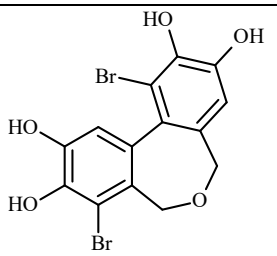

CPD-3 (20)	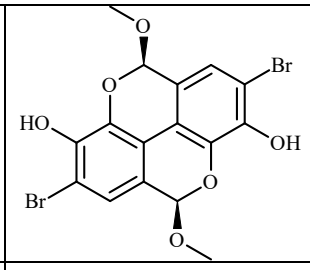	**CPD-4 (20)**	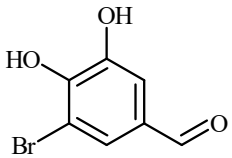
CPD-5 (20)	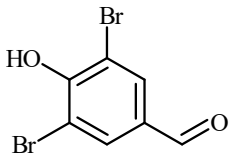	**CPD-6 (20)**	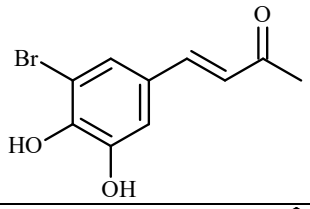
CPD-7 (21)	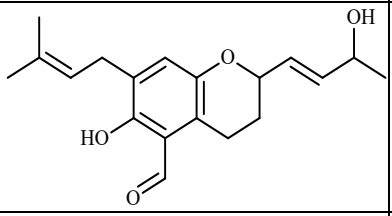	**CPD-8 (21)**	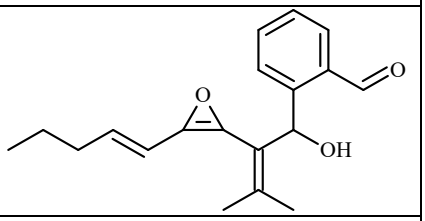
CPD-9 (21)	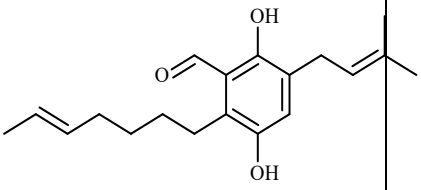	**CPD-10 (21)**	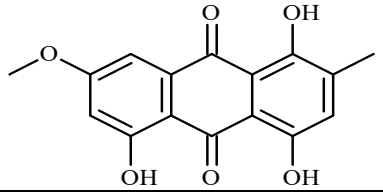
CPD-11 (22)	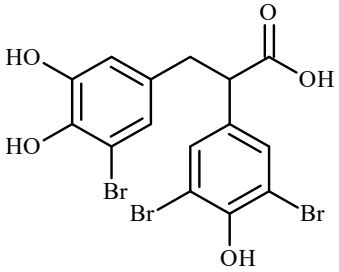	**CPD-12 (22)**	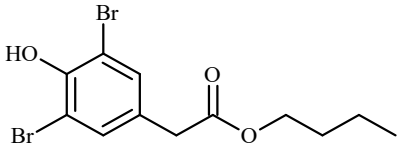
CPD-13 (22)	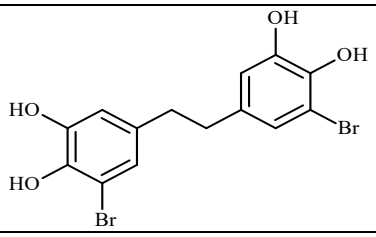	**CPD-14 (22)**	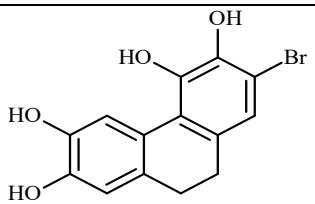
CPD-15 (22)	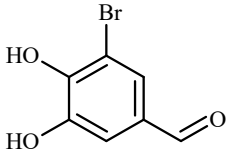	**CPD-16 (23)**	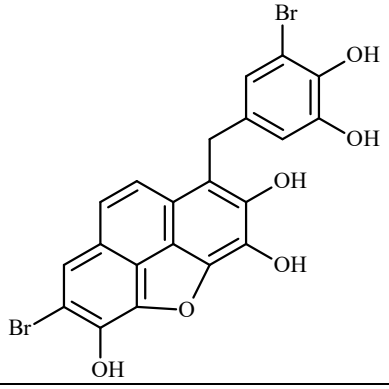

CPD-17 (24)	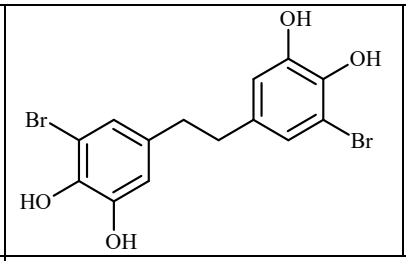	**CPD-18 (24)**	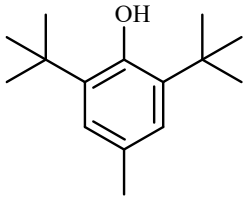
CPD-19 (28)	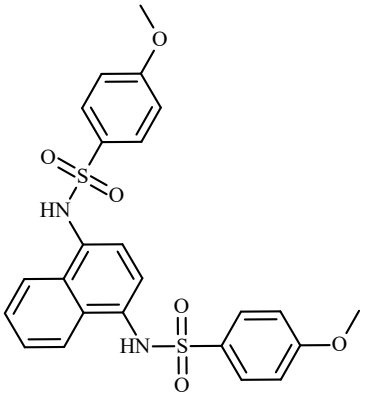		

3. RESULTS & DISCUSSION

Upon concluding the docking procedure, the results are ranked according to their binding affinity, with more negative values indicating better results **(Table.3.)**. The binding affinity differences between various ligands, in comparison to the cocrystallized ligand and the biological control, are calculated and presented in the table below. It is apparent from the results that CPD-16 (-11.0) demonstrated outstanding performance compared to all other test compounds, exhibiting a higher binding affinity than the cocrystallized ligand, with a difference exceeding 0.9 magnitude. In terms of biological control, the distinction is notably greater at a magnitude of 4.5. Consequently, based on the convergence quality, CPD-16 emerges as the optimal selection for subsequent investigations. Compounds such as CPD-10, 14, 1, 11, 2, 7, 13, 17, 8, 3, 9, and 6 are categorized as moderate, whereas CPD-12, 4, and 15 are regarded as the least favorable among the group. CPD-18 (2,6-Di-tert-butyl-4-methylphenol, BHT) is regarded as the biological control (baseline).

Table: 3. Binding affinity result of each compound along with differences with the co-crystal (CPD-16) and biological control (CPD-18, BHT) values in Kcal/mol

Rank	Ligand	Best Affinity (Kcal/mol)	Difference vs Co-crystal	Difference vs Biological Control	Convergence Quality
1	**4IQK Co-crystal**	-10.1	0.0	-	Excellent
2	**CPD-16**	-11.0	-0.9	-4.5	Excellent
3	**CPD-10**	-9.8	+0.3	-3.3	Moderate
4	**CPD-14**	-8.8	+1.3	-2.3	Moderate
5	**CPD-1**	-8.8	+1.3	-2.3	Moderate
6	**CPD-11**	-8.7	+1.4	-2.2	Moderate
7	**CPD-2**	-8.3	+1.8	-1.8	Moderate
8	**CPD-7**	-8.2	+1.9	-1.7	Moderate
9	**CPD-13**	-8.1	+2.0	-1.6	Moderate
10	**CPD-17**	-8.1	+2.0	-1.6	Moderate
11	**CPD-8**	-7.9	+2.2	-1.4	Moderate
12	**CPD-3**	-7.3	+2.8	-0.8	Moderate
13	**CPD-9**	-7.2	+2.9	-0.7	Moderate
14	**CPD-6**	-6.8	+3.3	-0.3	Moderate
15	**CPD-18**	-6.5	+3.6	0.0 (Baseline)	Moderate
16	**CPD-12**	-6.3	+3.8	+0.2	Weak
17	**CPD-4**	-6.1	+4.0	+0.4	Weak
18	**CPD-15**	-6.0	+4.1	+0.5	Weak
19	**CPD-5**	-5.6	+4.5	+0.9	Weak

We have cherry-picked the top four compounds and compared them with the co-crystallized ligand, considering its value as a baseline. CPD-16 outperforms co-crystal ligands with excellent convergence (RMSD=1.696 Å). CPD-10 is considered a strong hit but slightly less specific binding with higher RMSD (5.95 Å). CPD-14 and CPD-1 are considered

good hits, but CPD-1 (3.307 Å) has better specificity than CPD-14 (5.593 Å) as the RMSD is less than CPD-14 **(Table. 4)**.

Table:4. Top four compounds with their pose convergence w.r.t. 4IQK Co-crystal (mode 0 and mode 1)

Ligand	Best Affinity	IC_{50} in µM	ΔG vs Co-crystal	Pose Convergence (Mode 0 vs 1 RMSD)
4IQK Co-crystal	-10.1	7.9	0.0 (Baseline)	2.662 Å
CPD-16	-11.0	7.9	-0.9	1.696 Å
CPD-10	-9.8	62	+0.3	5.95 Å
CPD-14	-8.8	6.8	+1.3	5.593 Å
CPD-1	-8.8	6.1	+1.3	3.307 Å

The docking interactions of the protein-ligand bound complexes were analyzed based on the results from AutoDock Vina **(Table. 5)**. We are examining the leading four compounds listed in the Table.4.

Table. 5. Summary of the Protein-Ligand interactions of the complexes

Compound	Distance in Å	Category	From	From Chemistry	To	To Chemistry
CPD-16	2.6963	Hydrogen Bond	A:UNL1:O15	H-Donor	A:LEU365:O	H-Acceptor
	1.8996	Hydrogen Bond	A:GLY367:HN	H-Donor	A:UNL1:O6	H-Acceptor
	2.32215	Hydrogen Bond	A:UNL1:H5	H-Donor	A:VAL418:O	H-Acceptor
	2.1014	Hydrogen Bond	A:UNL1:H12	H-Donor	A:VAL606:O	H-Acceptor
	1.9475	Hydrogen Bond	A:UNL1:H11	H-Donor	A:LEU365:O	H-Acceptor
	4.20339	Hydrophobic	A:ALA466	Alkyl	A:UNL1:BR1	Alkyl
	4.61264	Hydrophobic	A:UNL1:BR2	Alkyl	A:ARG415	Alkyl
	4.27118	Hydrophobic	A:UNL1:BR1	Alkyl	A:VAL514	Alkyl
	5.16038	Hydrophobic	A:UNL1	Pi-Orbitals	A:ALA366	Alkyl
	4.265	Hydrophobic	A:UNL1	Pi-Orbitals	A:ALA366	Alkyl
	5.12634	Hydrophobic	A:UNL1	Pi-Orbitals	A:ALA366	Alkyl
CPD-10	2.83465	Hydrogen Bond	A:VAL465:HN	H-Donor	A:UNL1:O1	H-Acceptor
	1.76726	Hydrogen Bond	A:UNL1:H1	H-Donor	A:UNL1:O6	H-Acceptor
	1.79281	Hydrogen Bond	A:UNL1:H7	H-Donor	A:LEU365:O	H-Acceptor
	2.74631	Hydrogen Bond	A:UNL1:H12	H-Donor	A:VAL463:O	H-Acceptor
	1.83936	Hydrogen Bond	A:UNL1:H12	H-Donor	A:UNL1:O1	H-Acceptor
	3.55518	Hydrogen Bond	A:ALA366:CA	H-Donor	A:UNL1:O6	H-Acceptor
	3.42705	Hydrogen Bond	A:GLY464:CA	H-Donor	A:UNL1:O1	H-Acceptor
	3.39416	Hydrogen Bond	A:GLY605:CA	H-Donor	A:UNL1:O6	H-Acceptor
	4.96911	Hydrophobic	A:UNL1:C7	Alkyl	A:CYS513	Alkyl
	5.41273	Hydrophobic	A:UNL1:C7	Alkyl	A:ILE559	Alkyl
	4.79305	Hydrophobic	A:UNL1	Pi-Orbitals	A:ALA366	Alkyl
CPD-14	2.07038	Hydrogen Bond	A:VAL418:HN	H-Donor	A:UNL1:O2	H-Acceptor
	2.79152	Hydrogen Bond	A:UNL1:H7	H-Donor	A:VAL465:O	H-Acceptor
	2.26658	Hydrogen Bond	A:UNL1:H11	H-Donor	A:VAL463:O	H-Acceptor
	4.09857	Hydrophobic	A:ALA556	Alkyl	A:UNL1:BR1	Alkyl
CPD-1	2.2988	Hydrogen Bond	A:GLY367:HN	H-Donor	A:UNL1:O4	H-Acceptor
	3.0023	Hydrogen Bond	A:UNL1:H1	H-Donor	A:LEU365:O	H-Acceptor
	2.17586	Hydrogen Bond	A:UNL1:H7	H-Donor	A:LEU365:O	H-Acceptor
	2.17446	Hydrogen Bond	A:UNL1:H10	H-Donor	A:GLY367:O	H-Acceptor
	2.1269	Hydrogen Bond	A:UNL1:H10	H-Donor	A:VAL606:O	H-Acceptor
	2.47786	Hydrogen Bond	A:UNL1:H9	H-Donor	A:GLY367:O	H-Acceptor
	1.9221	Hydrogen Bond	A:UNL1:H9	H-Donor	A:VAL606:O	H-Acceptor

	4.06538	Hydrophobic	A:UNL1	Pi-Orbitals	A:ALA366	Alkyl

We have additionally examined the close contact residues of the compounds in addition with the compounds in CB-Dock2 (Table.6). Contact residues in CB-Dock2 refer to the amino acids on a protein that engage or interact physically with a bound ligand. CB-Dock2 detects these residues by automated blind docking to illustrate the binding of small molecules within a protein pocket. The CB-Dock2 close contact results indicate that the brominated polyphenolic chemical establishes an extensive interaction network within the conventional binding pocket of the Keap1 Kelch domain. This pocket is conventionally attributed for assisting the essential Keap1–Nrf2 protein–protein interaction. The outcomes align perfectly with the clearly defined sub-pockets (P1 to P5) that constitute the basic framework of the Keap1 Kelch domain.

Table: 6. List of contact residues of proteins along with the docked compounds

Compound ID	Contact residues
CPD-1	Chain A: TYR334 SER338 SER363 GLY364 LEU365 ALA366 GLY367 CYS368 ARG380 ASN382 ASN414 ARG415 ILE416 GLY417 VAL418 GLY462 VAL463 GLY464 VAL465 ALA466 ARG483 SER508 GLY509 ALA510 GLY511 VAL512 CYS513 GLY524 TYR525 GLN530 SER555 ALA556 LEU557 GLY558 ILE559 THR560 TYR572 PHE577 SER602 GLY603 VAL604 GLY605 VAL606 ALA607
CPD-2	Chain A: TYR334 SER338 SER363 GLY364 LEU365 ALA366 GLY367 CYS368 ARG380 ASN382 ASN414 ARG415 ILE416 GLY417 VAL418 GLY419 VAL420 ILE461 GLY462 VAL463 GLY464 VAL465 ALA466 GLY477 PHE478 ARG483 SER508 GLY509 ALA510 GLY511 VAL512 CYS513 TYR525 GLN530 SER555 ALA556 LEU557 GLY558 ILE559 THR560 VAL561 TYR572 PHE577 SER602 GLY603 VAL604 GLY605 VAL606 ALA607
CPD-3	Chain A: TYR334 SER363 GLY364 LEU365 ALA366 GLY367 ARG380 ASN382 ASN414 ARG415 ILE416 GLY417 VAL418 GLY419 VAL420 ILE461 GLY462 VAL463 GLY464 VAL465 ALA466 VAL467 PHE478 ARG483 SER508 GLY509 ALA510 GLY511 VAL512 CYS513 TYR525 GLN530 SER555 ALA556 LEU557 GLY558 ILE559 THR560 VAL561 TYR572 PHE577 SER602 GLY603 VAL604 GLY605 VAL606 ALA607 VAL608
CPD-4	Chain A: GLY333 TYR334 SER338 SER363 GLY364 LEU365 ALA366 GLY367 CYS368 ARG380 ASN382 ASN414 ARG415 ILE416 GLY417 VAL418 VAL463 GLY464 VAL465 ALA466 GLY509 ALA510 GLY511 VAL512 CYS513 ALA556 LEU557 GLY558 ILE559 THR560 TYR572 PHE577 SER602 GLY603 VAL604 GLY605 VAL606 ALA607
CPD-5	Chain A: SER363 GLY364 LEU365 ALA366 GLY367 ARG415 ILE416 GLY417 VAL418 GLY419 VAL420 GLY462 VAL463 GLY464 VAL465 ALA466 VAL467 SER508 GLY509 ALA510 GLY511 VAL512 CYS513 VAL514 ALA556 LEU557 GLY558 ILE559 THR560 VAL561 SER602 GLY603 VAL604 GLY605 VAL606
CPD-6	Chain A: TYR334 SER338 SER363 GLY364 LEU365 ALA366 GLY367 CYS368 GLY379 ARG380 ASN382 ASN414 ARG415 ILE416 GLY417 VAL418 ILE461 GLY462 VAL463 GLY464 VAL465 ALA466 SER508 GLY509 ALA510 GLY511 VAL512 CYS513 ALA556 LEU557 GLY558 ILE559 SER602 GLY603 VAL604 GLY605 VAL606 ALA607
CPD-7	Chain A: TYR334 SER338 SER363 GLY364 LEU365 ALA366 GLY367 CYS368 VAL369 ARG380 ASN382 ASN414 ARG415 ILE416 GLY417 VAL418 GLY419 VAL420 ILE461 GLY462 VAL463 GLY464 VAL465 ALA466 VAL467 PHE478 ARG483 SER508 GLY509 ALA510 GLY511 VAL512 CYS513 VAL514 TYR525 GLN530 SER555 ALA556 LEU557 GLY558 ILE559 THR560 TYR572 PHE577 SER602 GLY603 VAL604 GLY605 VAL606 ALA607 VAL608
CPD-8	Chain A: TYR334 SER363 GLY364 LEU365 ALA366 GLY367 CYS368 VAL369 ARG380 ASN382 ASN414 ARG415 ILE416 GLY417 VAL418 GLY419 VAL420 GLY462 VAL463 GLY464 VAL465 ALA466 VAL467 GLY509 ALA510 GLY511 VAL512 CYS513 VAL514 GLN530 SER555 ALA556 LEU557 GLY558 ILE559 THR560 VAL561 TYR572 PHE577 SER602 GLY603 VAL604 GLY605 VAL606 ALA607 VAL608
CPD-9	Chain A: TYR334 SER338 SER363 GLY364 LEU365 ALA366 GLY367 ARG380 ASN382 ASN414 ARG415 ILE416 GLY417 VAL418 ILE461 GLY462 VAL463 GLY464 VAL465 ARG483 SER508 GLY509 ALA510 GLY511 VAL512 TYR525 GLN530 SER555 ALA556 LEU557 GLY558 ILE559 TYR572 PHE577 SER602 GLY603 VAL604 GLY605 VAL606

CPD-10	Chain A: TYR334 SER338 SER363 GLY364 LEU365 ALA366 GLY367 CYS368 ARG380 ASN382 ASN414 ARG415 ILE416 GLY417 VAL418 GLY419 ILE461 GLY462 VAL463 GLY464 VAL465 ALA466 VAL467 ARG483 SER508 GLY509 ALA510 GLY511 VAL512 CYS513 TYR525 ALA556 LEU557 GLY558 ILE559 THR560 TYR572 PHE577 SER602 GLY603 VAL604 GLY605 VAL606 ALA607 VAL608
CPD-11	Chain A: TYR334 SER363 GLY364 LEU365 ALA366 GLY367 CYS368 ARG380 ASN382 ASN414 ARG415 ILE416 GLY417 VAL418 GLY419 VAL420 ILE461 GLY462 VAL463 GLY464 VAL465 ALA466 VAL467 PHE478 ARG483 SER508 GLY509 ALA510 GLY511 VAL512 CYS513 TYR525 GLN530 SER555 ALA556 LEU557 GLY558 ILE559 THR560 VAL561 GLY571 TYR572 PHE577 SER602 GLY603 VAL604 GLY605 VAL606 ALA607 VAL608
CPD-12	Chain A: TYR334 SER363 GLY364 LEU365 ARG380 ASN382 ASN414 ARG415 ILE416 ILE461 GLY462 VAL463 PHE478 ARG483 SER508 GLY509 ALA510 TYR525 GLN530 SER555 ALA556 TYR572 PHE577 SER602 GLY603
CPD-13	Chain A: TYR334 SER363 GLY364 LEU365 ALA366 GLY367 CYS368 ARG380 ASN382 ASN414 ARG415 ILE416 GLY417 VAL418 GLY419 ILE461 GLY462 VAL463 GLY464 VAL465 ALA466 PHE478 ARG483 SER508 GLY509 ALA510 GLY511 VAL512 CYS513 TYR525 GLN530 SER555 ALA556 LEU557 GLY558 ILE559 THR560 PHE577 SER602 GLY603 VAL604 GLY605 VAL606 ALA607
CPD-14	Chain A: SER363 GLY364 LEU365 ALA366 GLY367 CYS368 ARG415 ILE416 GLY417 VAL418 GLY419 VAL420 ILE421 GLY462 VAL463 GLY464 VAL465 ALA466 VAL467 GLY509 ALA510 GLY511 VAL512 CYS513 VAL514 ALA556 LEU557 GLY558 ILE559 THR560 SER602 GLY603 VAL604 GLY605 VAL606 ALA607
CPD-15	Chain A: TYR334 SER338 SER363 GLY364 LEU365 ALA366 GLY367 CYS368 GLY379 ARG380 ASN382 ASN414 ARG415 ILE416 GLY417 VAL418 GLY462 VAL463 GLY464 VAL465 ALA466 GLY509 ALA510 GLY511 VAL512 CYS513 ALA556 LEU557 GLY558 ILE559 GLY603 VAL604 GLY605 VAL606 ALA607
CPD-16	Chain A: GLY:333:A TYR334 SER363 GLY364 LEU365 ALA366 GLY367 CYS368 ARG380 ASN382 ASN387 ASN414 ARG415 ILE416 GLY417 VAL418 GLY419 VAL420 GLY462 VAL463 GLY464 VAL465 ALA466 VAL467 ARG483 SER508 GLY509 ALA510 GLY511 VAL512 CYS513 VAL514 TYR525 GLN530 SER555 ALA556 LEU557 GLY558 ILE559 THR560 VAL561 TYR572 PHE577 SER602 GLY603 VAL604 GLY605 VAL606 ALA607
CPD-17	Chain A: SER363 GLY364 LEU365 ALA366 GLY367 CYS368 ASN414 ARG415 ILE416 GLY417 VAL418 GLY419 ILE461 GLY462 VAL463 GLY464 VAL465 ALA466 SER508 GLY509 ALA510 GLY511 VAL512 CYS513 VAL514 ALA556 LEU557 GLY558 ILE559 THR560 VAL561 GLY603 VAL604 GLY605 VAL606 ALA607 VAL608
CPD-18 (BHT) Standard	Chain A: TYR334 SER363 GLY364 LEU365 ALA366 GLY367 ASN414 ARG415 ILE416 GLY417 VAL418 GLY419 VAL420 GLY462 VAL463 GLY464 VAL465 ALA466 VAL467 ARG483 SER508 GLY509 ALA510 GLY511 VAL512 CYS513 VAL514 TYR525 SER555 ALA556 LEU557 GLY558 ILE559 THR560 SER602 GLY603 VAL604 GLY605 VAL606 ALA607 VAL608
CPD-19 Control ligand 4IQK	Chain A: TYR334 SER363 GLY364 LEU365 ALA366 GLY367 ARG380 ASN382 ASN414 ARG415 ILE416 GLY417 VAL418 GLY419 ILE461 GLY462 VAL463 GLY464 VAL465 ALA466 VAL467 ARG483 SER508 GLY509 ALA510 GLY511 VAL512 CYS513 VAL514 TYR525 GLN530 SER555 ALA556 LEU557 GLY558 ILE559 THR560 VAL561 TYR572 PHE577 SER602 GLY603 VAL604 GLY605 VAL606 ALA607

3.1. Non-bonded interaction study of the four protein-ligand complexes

CPD-16 engages with the crucial residues ARG380, ASN382, ARG415, ASN414, and GLN530 **(Fig. 2)**. In the basic electrostatic sub-pockets (P1 & P2), these specific residues provide stabilization to acidic moieties (such as the carboxylates on Nrf2) within Keap1. In this context, these residues are probably interacting with the highly polarized hydroxyl (–OH) groups found on the polyphenolic rings of the ligands through strong hydrogen bonding networks. The residues TYR334, PHE577, TYR525, and TYR572 engage with the hydrophobic/aromatic sub-pocket (P3). These residues constitute the base and sides of the core hydrophobic cavity (tunnel) and will engage in π-π stacking and hydrophobic interactions with the aromatic rings and the significant bromine (Br) substituents of the ligand. In the Flexible Glycine-Rich Loops (P4 & P5), the ligand demonstrates intense contact clusters among several glycine/valine motifs

(GLY364–GLY367, VAL418–VAL420, GLY462–VAL467, GLY509–VAL514, and GLY603–ALA607). These areas represent the intricately structured, flexible loops that surround the Kelch blades, securing the ligand tightly.

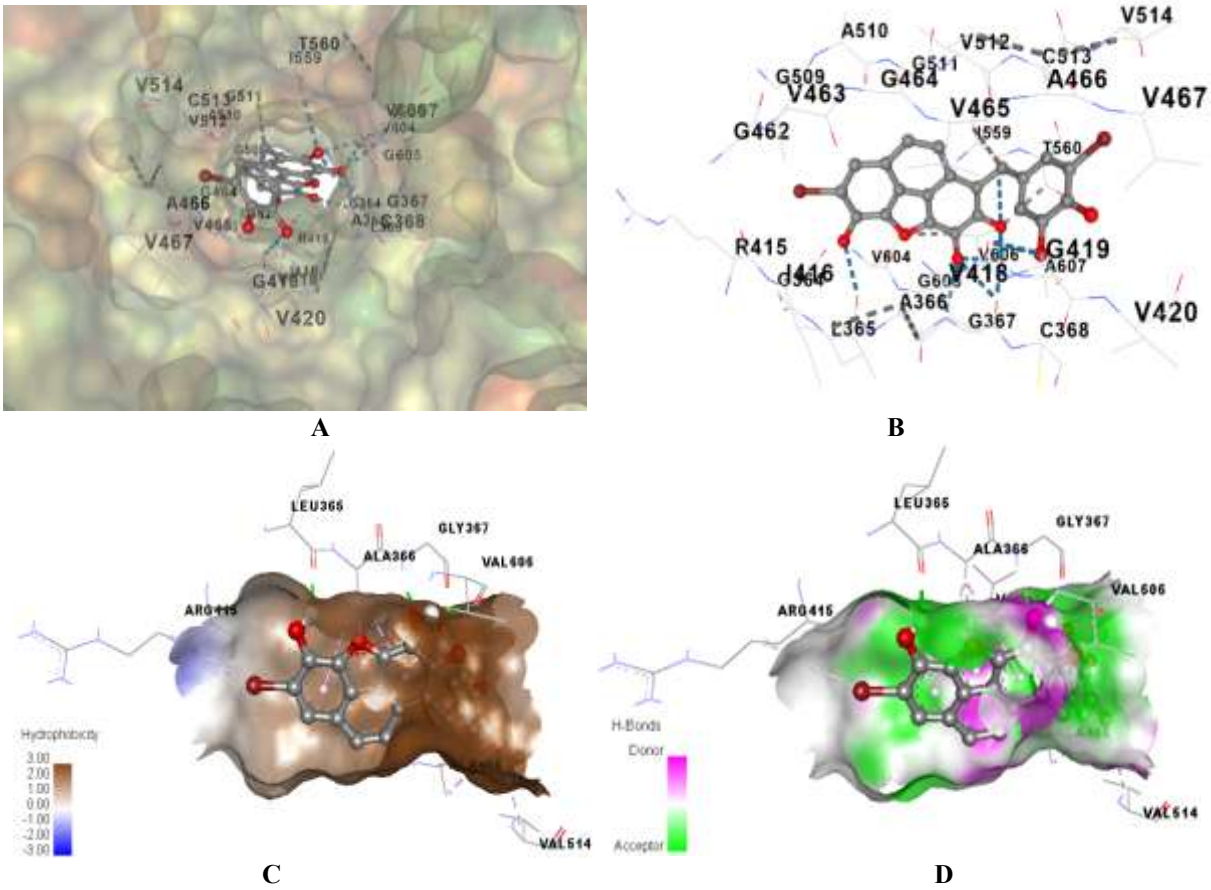

Fig. 2. A. Interaction of **CPD-16** (hydrogen suppressed) with the amino acid residues of the protein (surface) in close contact; B. Interaction without the receptor surface; **C.** Important hydrophobic interaction of the ligand atoms with the contact residues; **D.** Hydrogen bond interaction of the ligand atoms with the contact residues.

The presence of ARG415, ARG380, and ASN382 in the contact results is greatly significant. These are the conventional anchoring residues that potent Keap1-Nrf2 small-molecule inhibitors aim to target. Their morphology suggests that the docked ligand configuration is probably attaining a biologically relevant binding orientation capable of displacing Nrf2. Through the assessment of the biochemical characteristics of the proximate residues, the brominated polyphenolic ligand employs a dual-mode stabilizing mechanism via hydrogen bonding and polar interactions. The molecule possesses many hydrophilic hydroxyl (–OH) groups that interact with the basic and polar regions of the Keap1 cavity through electrostatic networks. CPD-16 engages with arginine anchors (ionic interactions / hydrogen bonds) such as ARG380, ARG415, and ARG483. These are the most essential electrostatic residues within the Keap1 pocket. They generally establish robust salt bridges or oriented hydrogen bonds with the ligand's negatively charged or polar areas. Polar amides and hydrate remnants ASN382, ASN387, ASN414, and GLN530 delineate the P2 and P5 sub-pockets, thereby reinforcing the surrounding hydroxyl networks of the ligand. The residues SER363, SER555, and THR560 are regarded as serine/threonine anchors, presenting side-chain hydroxyl groups for direct hydrogen bonding. The chemical features a significantly hydrophobic, halogenated nucleus including numerous aromatic rings and bromine atoms. It is maintained by the subsequent residue clusters, the aromatic π- The residues that are stacked are TYR334, TYR525, TYR572, and PHE577. These remnants create planar, hydrophobic surfaces. They are situated to engage in direct or edge-to-edge π-π interactions with the polyphenolic rings. The nonpolar side chains such as LEU365, ILE416, VAL418, VAL420, VAL463, VAL465, VAL467, VAL512, VAL514, LEU557, ILE559, VAL561, and VAL606 encircle the core, creating a hydrophobic enclosure that secures the ligand. The amino acids GLY333, GLY364, GLY367, GLY417, GLY419, GLY462, GLY464, GLY509, GLY511, GLY558, GLY603, and GLY605 create structural pivots that enable close conformational enclosure around the substantial bromine atoms.

CPD-10 features a rigid, planar aromatic core decorated with two ketone groups (C=O), three hydroxyl groups (–OH), a methoxy group (–OCH_3), and a methyl group (–CH_3) (Fig. 3). This scaffold is more compact, highly rigid, and less bulky than CPD-16. The oxygen-rich topology of this molecule (ketones and phenols) forms strong, directional networks with the basic and polar sub-pockets of Keap1. The two central ketone groups (C=O) act as strong hydrogen bond acceptors. They unidirectionally coordinate and anchor with the ARG415 and ARG380 residues (the primary electrostatic anchors of the P1 and P2 sub-pockets). The three hydroxyl groups (–OH) serve as both peripheral H-bond donors and acceptors,

interacting with polar amide side chains like ASN382, ASN414, and GLN530. The molecule's planar edges can readily form stable bridges with the hydroxyl clusters of SER363, SER508, and SER555.

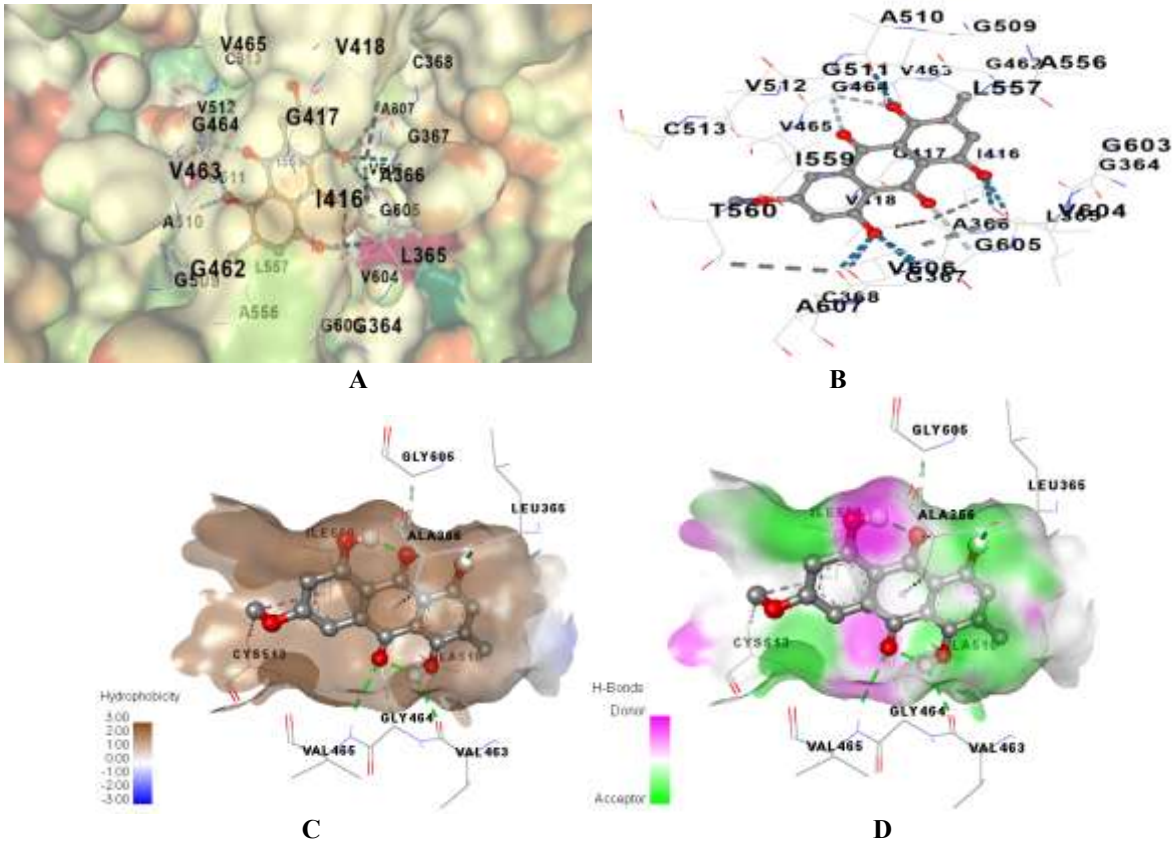

Fig. 3. A. Interaction of **CPD-10** (hydrogen suppressed) with the amino acid residues of the protein in close contact; B. Interaction without the receptor surface; **C.** Important hydrophobic interaction of the ligand atoms with the contact residues; **D.** Hydrogen bond interaction of the ligand atoms with the contact residues.

CPD-14 represents a semi-rigid, bridged brominated polyphenolic compound **(Fig. 4)**. It features four phenolic hydroxyl groups (–OH), a heavy bromine atom (Br), and a central partially rigidified ring junction (CC bridge) linking the aromatic systems. This compound combines the beneficial features of the first two molecules, and it retains the heavy halogen anchoring of the CPD-16 while incorporating a more rigidized core system. The four outer hydroxyl groups act as a polar canopy, allowing the molecule to establish an extensive network of hydrogen bonds. The terminal phenolic –OH groups act as strong hydrogen bond donors to coordinate directly with ARG415, ARG380, and ARG483 residues within the P1 and P2 sub-pockets to form an electrostatic anchor. The broad distribution of hydroxyl groups allows it to participate in widespread H-bonding with surrounding polar residues such as ASN382, ASN414, ASN387, and GLN530. The oxygen atoms readily establish directional hydrogen bonds with the side-chain hydroxyls of SER363 and SER555, forming the serine-rich loop binding core. The molecule presents a unique architecture combining aromatic rings, a bulky bromine atom, and a fused aliphatic linker to form hydrophobic & π- Stacking contacts. The heavy, polarizable bromine (Br) atom is ideally suited to nestle into the deep hydrophobic cleft or engage in halogen-bonding interactions near PHE577, TYR572, or TYR334, forming an excellent bromine-halogen-pocket fitting. The aromatic rings engage in face-to-face or edge-to-face π-π stacking interactions with the classic aromatic floor residues (TYR334, TYR525, and TYR572). The non-aromatic carbon bridging segment fits snugly against the non-polar, aliphatic side chains of residues like VAL418, VAL465, ILE416, and LEU557 (the P3 sub-pocket). Flexible loops containing GLY364, GLY462, and GLY603 fold over and contour around the central bridging section of the ligand to lock its pose in place.

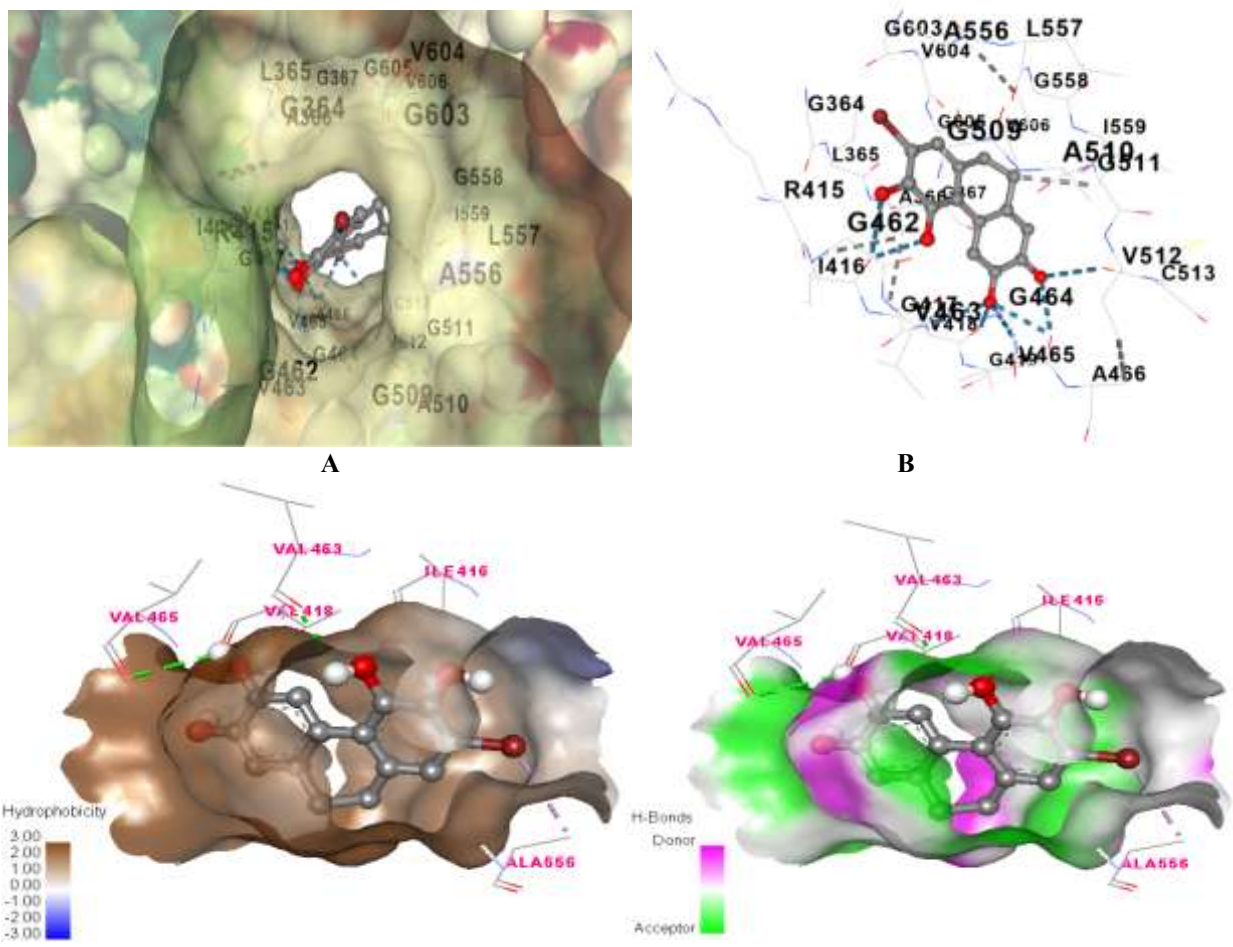

Fig. 4. A. Interaction of **CPD-14** (hydrogen suppressed) with the amino acid residues of the protein in close contact; B. Interaction without the receptor surface; **C.** Important hydrophobic interaction of the ligand atoms with the contact residues; **D.** Hydrogen bond interaction of the ligand atoms with the contact residues.

CPD-1 represents a dibrominated, highly rigid polycyclic polyphenolic derivative **(Fig. 5).** Compared to CPD-14, it has a second heavy bromine atom (Br) directly attached to the first aromatic ring cluster. This creates a highly symmetrical, heavily halogenated, and electron-deficient aromatic system. This specific topology maximizes halogen bonding and hydrophobic packing within the Keap1 Kelch domain. The addition of the second bromine atom significantly increases the acidity of the neighboring phenolic hydroxyl groups (–OH), making them stronger hydrogen bond donors. The highly polarized –OH groups engage in remarkably strong, directional hydrogen bonds with the primary pocket anchors ARG415, ARG380, and ARG483; this enhances arginine-coordinating anchors. The outer oxygen atoms maintain highly stable coordination with the polar side chains of ASN382, ASN414, and GLN530, which helps in peripheral amide trapping. Direct, multi-point polar interactions are formed along the peptide backbones and side chains of SER363, SER508, and SER555 that accelerate serine ribbon binding. The defining characteristic of this molecule is its dual-halogen footprint, which allows it to concurrently exploit two distinct lipophilic sub-pockets. With two bulky, polarizable bromine (Br) atoms, this ligand can simultaneously occupy both the P3 and P4 sub-pockets. These heavy atoms form highly specific directional halogen bonds with the carbonyl backbones of loop residues. The core fused ring system slips into the central hydrophobic cleft of the Kelch domain, forming strong face-to-face π-π interactions with TYR334, TYR525, TYR572, and PHE577. The central carbon bridging junction (CC) packs closely against non-polar side chains like VAL418, VAL465, ILE416, and LEU557. The dense clusters of glycine residues (GLY364, GLY462, GLY509, and GLY603) form a flexible cage that contours tightly around the bulky dibrominated scaffold. A summary of all the important interactions is cited in the table **(Table. 7)**.

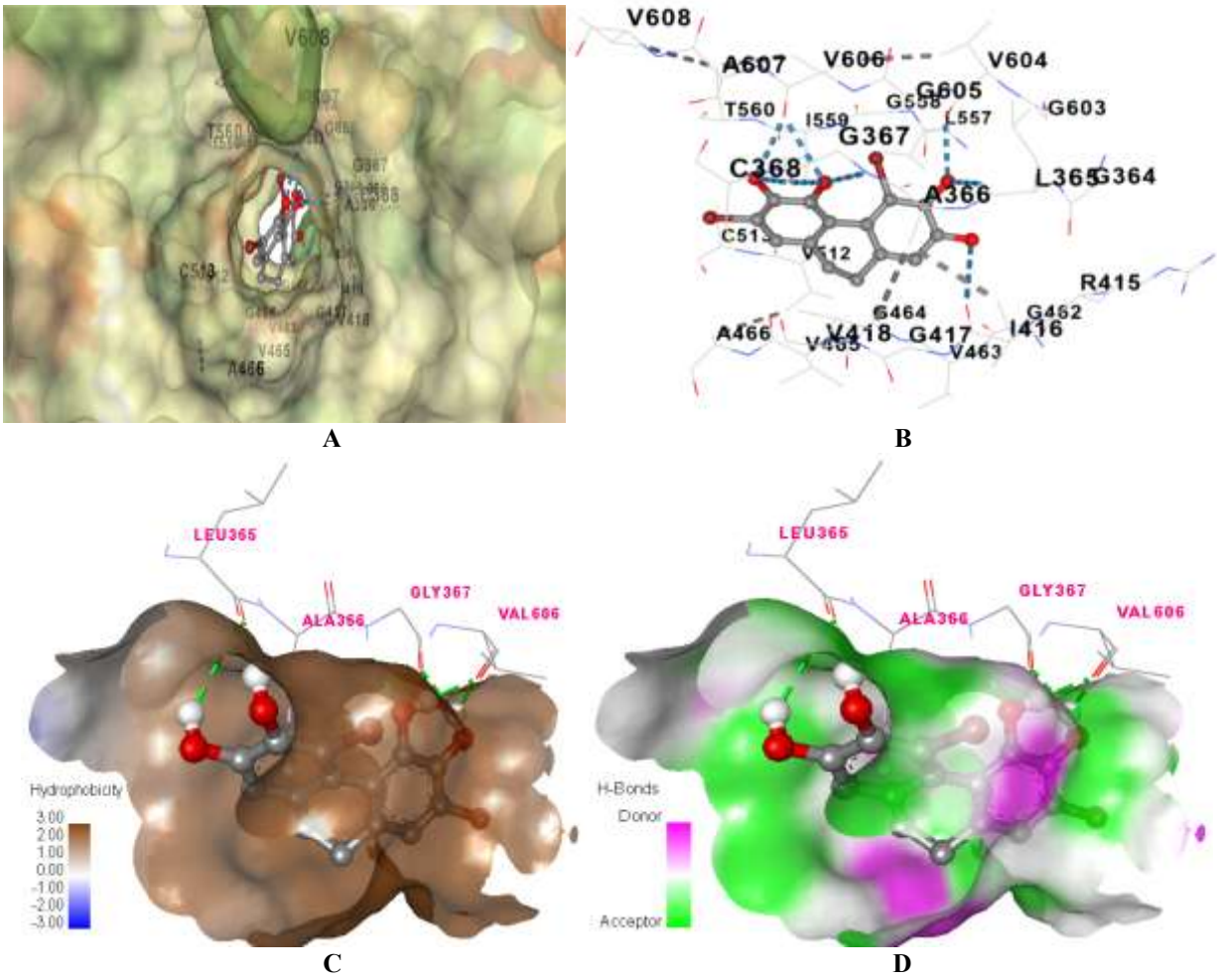

Fig. 5. A. Interaction of **CPD-1** (hydrogen suppressed) with the amino acid residues of the protein in close contact; **B.** Interaction without the receptor surface; **C.** Important hydrophobic interaction of the ligand atoms with the contact residues; **D.** Hydrogen bond interaction of the ligand atoms with the contact residues.

Table. 7. A summary of comparative study of the interactions four compounds with the protein

Compound	Binding Score	H-Bonds	H-Bond Partners	Hydrophobic Contacts
CPD-16	-11.0	4	GLY367, VAL418, VAL606, LEU365	BR1→ALA466, BR2→ARG415, BR1→VAL514, Pi→ALA366 (x3)
CPD-10	-9.8	8	VAL465, LEU365, VAL463, GLY464, GLY605	C7→CYS513/ILE559, Pi→ALA366
CPD-14	-8.8	3	VAL418, VAL465, VAL463	BR1→ALA556
CPD-1	-8.8	7	GLY367, LEU365, GLY367, VAL606	Pi→ALA366

3.2. Compliance of the compounds with Lipinski's rule of five (RO5)

The Lipinski's rule of five was evaluated, revealing a single violation in CPD-16 **(Table. 8)**. The molecular weight threshold is set at 500 Dalton; however, in CPD-16, it was shown to exceed this threshold slightly at 520 Dalton. Lipinski's rule of five serves as a guideline to assess if a chemical compound possesses adequate physical and chemical characteristics to function as an orally drug in humans. It indicates that a drug-like compound often contains at most one violation of four fundamental criteria, all of which pertain to numerical values associated with the number five.

Table. 8. The molecular descriptor values of all the compounds were calculated for Lipinski's rule of five (RO5)

Compound ID	Nomenclature	IC_{50} in µM	Molecular Weight (g/mol)	Consensus Log Po/w	No. of Hbond Acceptors	No. of Hbond Donors	No. of Rotatable Bonds	Drug likeness Lipinski
CPD-1	4,7-dibromo-9,10-dihydrophenanthrene-2,3,5,6-tetraol	6.1	402.03	3.45	4	4	0	0 violation

CPD-2	1,8-dibromo-5,7-dihydrodibenzo[c,e]oxepine-2,3,9,10-tetraol	8.1	418.03	2.78	5	4	0	0 violation
CPD-3	(5R,10R)-2,7-dibromo-5,10-dimethoxy-5,10-dihydrochromeno[5,4,3-cde]chromene-3,8-diol (Urceolatol)	9	460.07	3.24	6	2	2	0 violation
CPD-4	3-Bromo-4,5-dihydroxybenzaldehyde	9.9	217.02	1.42	3	2	1	0 violation
CPD-5	3,5-Dibromo-4-hydroxybenzaldehyde	35.8	279.91	2.69	2	1	1	0 violation
CPD-6	(E)-4-(3-bromo-4,5-dihydroxyphenyl)-but-3-en-2-one	10.3	257.08	2.13	3	2	2	0 violation
CPD-7	6-hydroxy-2-((E)-3-hydroxybut-1-enyl)-7-(3-methylbut-2-enyl)-3,4-dihydro-2H-chromene-5-carbaldehyde; 6-hydroxy-2-[(E)-3-hydroxybut-1-enyl]-7-(3-methylbut-2-enyl)-3,4-dihydro-2H-chromene-5-carbaldehyde (Chaetopyranin)	35	316.39	3.41	4	2	5	0 violation
CPD-8	2-(2′,3-epoxy-1′,3′-heptadienyl)-6-hydroxy-5-(3-methyl-2-butenyl) benzaldehyde	88	298.38	3.88	3	1	7	0 violation
CPD-9	2-[(E)-hept-5-enyl]-3,6-dihydroxy-5-(3-methylbut-2-enyl)benzaldehyde (Isotetrahydroauroglaucin	26	302.41	4.80	3	2	8	0 violation
CPD-10	1,4,5-trihydroxy-7-methoxy-2-methylanthracene-9,10-dione (Erythroglaucin)	62	300.26	1.95	6	3	1	0 violation
CPD-11	3-(3-bromo-4,5-dihydroxyphenyl)-2-(3,5-dibromo-4-hydroxyphenyl)propionic acid	21.9	510.96	4.09	5	4	4	0 violation
CPD-12	(3,5-dibromo-4-hydroxyphenyl)acetic acid butyl ester	16.11	366.05	3.86	3	1	6	0 violation
CPD-13	1,2-bis(3-bromo-4,5-dihydroxyphenyl)ethane	19.64	404.05	3.64	4	4	3	0 violation
CPD-14	7-bromo-9,10-dihydrophenanthrene-2,3,5,6-tetraol	6.8	323.14	2.76	4	4	0	0 violation
CPD-15	5-Bromo-3,4-dihydroxybenzaldehyde	20.29	217.02	1.42	3	2	1	0 violation
CPD-16	6-Bromo-1-(3-bromo-4,5-dihydroxybenzyl)phenanthro[4,5-bcd]furan-2,3,5-triol (urceolatin)	7.9	520.12	4.87	6	5	2	Yes; 1 violation: MW>500
CPD-17	3-bromo-5-[2-(3-bromo-4,5-dihydroxyphenyl)ethyl]benzene-1,2-diol	19.64	404.05	3.64	4	4	3	0 violation
CPD-18	BHT (Positive Control) 2,6-Di-tert-butyl-4-methylphenol	83.8	220.35	4.46	1	1	2	0 violation
CPD-19	N,N′-Naphthalene-1,4-diylbis(4-methoxybenzenesulfonamide)	7.9	498.57	3.75	6	2	8	0 violation

3.3. Common Feature Pharmacophore

All four compounds (CPD-16, 10, 14, and 1) are polyphenolic, with many phenolic hydroxyl (-OH) groups linked to their aromatic ring structures. The presence and configuration of these hydroxyl groups are essential for their potential to scavenge free radicals. A vital feature is the existence of catechol or pyrogallol. This configuration is an insignia of powerful antioxidant pharmacophores. Every compound comprises a minimum of one bromine atom. The presence and positions of these halogens are crucial for influencing the compound's biological efficacy and strength. Three of the compounds are derived from a phenanthrene scaffold, while the other is a derivative of anthracene. This establishes a firm, flat structure for the pharmacophore.

CONCLUSION

From the present study, it can be inferred that out of these seventeen compounds under study, one compound, CPD-16 (6-Bromo-1-(3-bromo-4,5-dihydroxybenzyl)phenanthro[4,5-bcd]furan-2,3,5-triol) (urceolatin), was found to outperform the co-crystallized inhibitor available in the protein data bank. The compound is likely to behave analogously to that of the co-crystallized ligand, i.e., N,N′-Naphthalene-1,4-diylbis(4-methoxybenzenesulfonamide), and could be an effective inhibitor of the protein-protein interaction between NRF2 and KEAP1 (Kelch-like ECH-associated protein 1). Inhibiting this interaction in humans may augment free radical scavenging activity, and several diseases can be controlled. The remaining three compounds are also worth mentioning, as the IC_{50} values and the docking results are satisfactory enough for future studies as individual compounds. As it is beyond the scope of our present work, subsequent investigations on protein-protein inhibition studies are necessary to validate the hypothesis derived in this research.

ACKNOWLEDGMENTS

The authors express their gratitude to the institution and university departments for their technical and moral assistance in successfully carrying out the project.

AUTHORS' CONTRIBUTIONS

All the authors have contributed equally.

CONFLICTS OF INTEREST

The authors declare that there are no conflicts of interest.

FUNDING

The projected was completely funded by the authors.

REFERENCES

1. Chandimali N, Bak S.G, Park E.H, Free radicals and their impact on health and antioxidant defenses: a review. Cell Death Discov. 2025 Jan;11(1):19.https://doi.org/10.1038/s41420-024-02278-8
2. Jomova K, Raptova R, Alomar S.Y, Reactive oxygen species, toxicity, oxidative stress, and antioxidants: chronic diseases and aging. Arch Toxicol.2023;97(10):2499-2574. https://doi.org/10.1007/s00204-023-03562-9
3. Lobo V, Patil A, Phatak A, Chandra N. Free radicals, antioxidants and functional foods: Impact on human health. Pharmacogn Rev.2010;4(8):118-126. https://doi.org/10.4103/0973-7847.70902
4. Aladhadh M. Antioxidants: Mechanisms, Benefits, and the Importance of Extremophilic Microorganisms. Microorganisms.2026 Apr 8,14(4):823. https://doi.org/10.3390/microorganisms14040838
5. Wong E, Cuervo AM. Integration of clearance mechanisms: the proteasome and autophagy. Cold Spring Harb Perspect Biol.2010;2(12): a006734. https://doi.org/10.1101/cshperspect.a006734
6. Yin C, Heit B. Cellular Responses to the Efferocytosis of Apoptotic Cells. Front Immunol. 2021 Apr 20;12: 631714. https://doi.org/10.3389/fimmu.2021.631714
7. Kalyanaraman B. Teaching the basics of redox biology to medical and graduate students: Oxidants, antioxidants and disease mechanisms. Redox Biol.2013 Feb 8;1(1):244-257.https://doi.org/10.1016/j.redox.2013.01.014
8. Irshad M, Chaudhuri PS. Oxidant-antioxidant system: role and significance in human body. Indian J Exp Biol.,2002;40(11):1233-1239
9. Handy DE, Loscalzo J. Redox regulation of mitochondrial function. Antioxid Redox Signal.2012;16(11):1323-1367. https://doi.org/10.1089/ars.2011.4123
10. Waris G, Ahsan H. Reactive oxygen species: role in the development of cancer and various chronic conditions. J Carcinog.2006 May 11;5:14. https://doi.org/10.1186/1477-3163-5-14
11. Chen X, Xie N, Feng L, et al. Oxidative stress in diabetes mellitus and its complications: From pathophysiology to therapeutic strategies. Chin Med J (Engl).2025;138(1):15-27. https://doi.org/10.1097/CM9.0000000000003230
12. Jankó, L., Tóth, E., Laczik, M. et al. PARP2 poly (ADP-ribosyl) ates nuclear factor erythroid 2-related factor 2 (NRF2) affecting NRF2 subcellular localization. Sci Rep. 2023; 13:7869. https://doi.org/10.1038/s41598-023-35076-w
13. Kobayashi A, Kang MI, Okawa H, et al. Oxidative stress sensor Keap1 functions as an adaptor for Cul3-based E3 ligase to regulate proteasomal degradation of Nrf2. Mol Cell Biol. 2004;24(16):7130-7139. https://doi.org/10.1128/MCB.24.16.7130-7139.2004
14. Espinosa-Diez C, Miguel V, Mennerich D, et al. Antioxidant responses and cellular adjustments to oxidative stress. Redox Biol.2015; 6:183-197. https://doi.org/10.1016/j.redox.2015.07.008

15. Zoccarato A, Smyrnias I, Reumiller CM, et al. NRF2 activation in the heart induces glucose metabolic reprogramming and reduces cardiac dysfunction via upregulation of the pentose phosphate pathway. Cardiovasc Res.2025;121(2):339-352. https://doi.org/10.1093/cvr/cvae250
16. He F, Ru X, Wen T. NRF2, a Transcription Factor for Stress Response and Beyond. Int J Mol Sci. 2020 july;21(13):4777. https://doi.org/doi:10.3390/ijms21134777
17. Choudhury R and Sahoo N, Phytochemical Evaluation and Bioactivity of Polysiphonia subtilissima Montagne. Asian journal of chemistry.2024 Aug;6(9):2083. https://doi.org/10.14233/ajchem.2024.32122
18. Choudhury R, Sahoo N, and Kar N.R. Identification of the isolated components and study of antifungal and anticancer activity of the extracts of Polysiphonia Subtilissima Montagne. Asian Pharmaceutical and Journal of Clinical Research.2025;18(10):126-146. https://doi.org/10.22159/ajpcr.2025v18i10.55606
19. Choudhury R, Sahoo N, and Kar N.R. Marine Bromophenols from polysiphonia: structural features, biological activity correlations, and future therapeutic applications, Genetics, and molecular research, 2026 june;25(8s).https://doi.org/10.4238/q3cacm35.
20. Li K, Li XM, Ji NY, Wang BG. Bromophenols from the marine red alga Polysiphonia urceolata with DPPH radical scavenging activity. J Nat Prod.2008;71(1):28-30. https://doi.org/10.1021/np070281p
21. Wang S, Li XM, Teuscher F, et al. Chaetopyranin, a benzaldehyde derivative, and other related metabolites from Chaetomium globosum, an endophytic fungus derived from the marine red alga Polysiphonia urceolata. J Nat Prod.2006;69(11):1622-1625. https://doi.org/10.1021/np060248n
22. Li K, Li XM, Ji NY, Wang BG. Natural bromophenols from the marine red alga *Polysiphonia urceolata* (Rhodomelaceae): structural elucidation and DPPH radical-scavenging activity. Bioorg Med Chem.2007;15(21):6627-6631. https://doi.org/10.1016/j.bmc.2007.08.023
23. Li K, Li XM, Ji NY, Gloer JB, Wang BG. Urceolatin, a structurally unique bromophenol from Polysiphonia urceolata. Org Lett.2008;10(7):1429-1432. https://doi.org/10.1021/ol800230t
24. Golmakani MT, Alavi SN, Sabet Sarvestani F, Shaabani S, Ibáñez E. Seaweed phenolic compounds: Relationship with antioxidant activity and application in different food products. Food Chem X.2025 Nov; 32:103242. https://doi.org/10.1016/j.fochx.2025.103242
25. Chemical Structure Drawing Standard; Cambridge Soft Corporation: USA, 2010
26. Daina A, Michielin O, Zoete V. SwissADME: a free web tool to evaluate pharmacokinetics, drug-likeness and medicinal chemistry friendliness of small molecules. Sci Rep.2017 Mar; 7:42717. https://doi.org/10.1038/srep42717
27. Lipinski CA. Lead- and drug-like compounds: the rule-of-five revolution. Drug. Discov. Today Technol.2004; 1(4):337-341. https://doi.org/10.1016/j.ddtec.2004.11.007
28. Marcotte. D, Zeng.W, Hus. J.C, McKenzie A, Hession C, Jin P, Bergeron C, Lugovskoy A, Enyedy I, Cuervo H, Wang D, Atmanene C, Roecklin D, Vecchi M, Vivat V, Kraemer J, Winkler D, Hong V, Chao J, Lukashev M, Silvian L, Small molecules inhibit the interaction of Nrf2 and the Keap1 Kelch domain through a non-covalent mechanism, Bioorganic & Medicinal Chemistry.2013;21(14):4011-4019, ISSN 0968-0896, https://doi.org/10.1016/j.bmc.2013.04.019
29. Morris GM, Huey R, Lindstrom W, et al. AutoDock4 and AutoDockTools4: Automated docking with selective receptor flexibility. J Comput Chem. 2009;30(16):2785-2791. https://doi.org/10.1002/jcc.21256
30. Liu Y, Yang X, Gan J, Chen S, Xiao ZX, Cao Y. CB-Dock2: improved protein-ligand blind docking by integrating cavity detection, docking and homologous template fitting. Nucleic Acids Res.2022;50(W1):W159-W164. https://doi.org/10.1093/nar/gkac394
31. Padmanabhan B, Tong KI, Ohta T, et al. Structural basis for defects of Keap1 activity provoked by its point mutations in lung cancer. Mol Cell. 2006;21(5):689-700. https://doi.org/10.1016/j.molcel.2006.01.013